

Spin-selective elliptic optical dichroism and perfectly spin-polarized third-order nonlinear photocurrent in altermagnets

Motohiko Ezawa¹

¹*Department of Applied Physics, The University of Tokyo, 7-3-1 Hongo, Tokyo 113-8656, Japan*
(Dated: March 10, 2026)

It is shown that the low-energy theory of a d -wave altermagnet is characterized by anisotropic Dirac cones with up and down spins based on a recently proposed tight-binding model. Spin-selective perfect elliptic dichroism occurs in this system, where only up-spin or down-spin electrons are excited by elliptically polarized light. Then, we derive a formula for the third-order photocurrent induced by applying both elliptically polarized light and static electric field, which is described in terms of quantum metric and the Berry curvature. Based on it, we predict only up-spin polarized current is induced. It is the leading order of photocurrent because the second-order photocurrent such as the injection current and the shift current are prohibited due to inversion symmetry inherent to altermagnets. It is intriguing that nonzero photocurrent is induced only by the anisotropy of the Dirac cones. Our results will be useful for future photo-excited spintronics based on altermagnets.

Introduction: Altermagnets[1, 2] are one of the hottest topics in condensed matter physics because they will be useful for future spintronics applications. They are collinear antiferromagnets but break time reversal symmetry, which allows nonzero anomalous Hall effect. Especially, d -wave altermagnets are prominent, where spin currents are induced by electric field[3–8] and temperature gradient[3, 8]. d -wave altermagnets have a combinatorial symmetry of time-reversal symmetry and the four-fold rotational symmetry[1, 2]. This symmetry enforces a spin-split band structure. In addition, altermagnets have inversion symmetry. There is a simple four-band tight-binding model possessing all these symmetry properties of d -wave altermagnets and confirmed by the density-functional theory[9].

Circular dichroism is an intriguing phenomenon, which was originally proposed in honeycomb systems[10–13]. The tight-binding model based on the honeycomb lattice possesses two Dirac cones assigned by different valley degrees of freedom. By irradiating circularly-polarized light to the system, only electrons at one valley are excited. Furthermore, circular dichroism is generalized to elliptic dichroism for anisotropic Dirac cones[8, 14, 15], where only one valley is excited by irradiating elliptically-polarized light. Elliptic dichroism is formulated in terms of quantum metric and the Berry curvature[8, 15].

The leading-order of photo-induced current is the second order in electric field, i.e., $j \propto E^2$, where there are injection current[16–25] and the shift current[16–20, 23–33]. However, they are prohibited if the system has inversion symmetry because current and electric field are odd under inversion symmetry. Hence, there is no second-order photocurrent in altermagnets. On the other hand, the third-order photocurrent $j \propto E^3$ is allowed even in the presence of inversion symmetry. A typical example is the jerk current[34–38], which has been discussed so far only for linearly polarized light.

In this paper, we derive a low-energy theory of altermagnets, which is characterized by anisotropic Dirac cones. Based on it, we show that elliptic dichroism occurs in altermagnet, where only electrons with up or down spin are excited by suitably tuning the ellipticity of the irradiating light. In addition, we derive for the first time a formula for higher-order pho-

tocurrent under elliptically polarized light, which we express in terms of quantum metric and the Berry curvature as in the case of the formula for the elliptic optical dichroism. Then, we predict that the perfectly spin-polarized third-order photocurrent is induced by applying elliptically polarized light and static electric field simultaneously. Our results will be useful for future photo-excited spintronics based on altermagnets.

Model: We start with the four-band tight-bind model for d -wave altermagnets defined on the square lattice[9, 39, 40],

$$\begin{aligned}
 H = & (\mu + A(\cos k_x + \cos k_y))\tau_0\sigma_0 \\
 & + B(\cos k_x - \cos k_y)\tau_z\sigma_0 \\
 & + t\cos\frac{k_x}{2}\cos\frac{k_y}{2}\tau_x\sigma_0 + \lambda\sin\frac{k_x}{2}\sin\frac{k_y}{2}\tau_y\sigma_z \\
 & + C(\cos k_x - \cos k_y)\tau_0\sigma_z \\
 & + (u + D(\cos k_x + \cos k_y))\tau_z\sigma_z, \quad (1)
 \end{aligned}$$

where σ_j is the Pauli matrix for the spin, τ_j is that for the sublattice degrees of freedom with $j = x, y, z$. u is a real number proportional to the spin order, and μ is the chemical potential. A and B are the isotropic and anisotropic hoppings of the next-nearest neighbor sites, while C and D are the isotropic and anisotropic spin-dependent hoppings of the next-nearest neighbor sites. t is the hopping and λ is the spin-dependent hopping of nearest-neighbor sites. We assume $t > 0$ and $\lambda > 0$. The model was derived from the Lieb lattice as shown in Fig.1(a).

Because σ_z is a good quantum number, we may set $\sigma_z = s$ with $s = \pm 1$ in the Hamiltonian (1). Then, the Hamiltonian is reduced to a direct sum of two two-band models, $H = H_\uparrow \oplus H_\downarrow$. The band structure is shown in Fig.1(b) and (c). With respect to the band with up spin $s = 1$, there is a Dirac cone at the X point, where the Hamiltonian is expanded as

$$H_\uparrow^X = -4C + tk'_x\tau_x + \lambda k_y\tau_y - (4B - 2u)\tau_z \quad (2)$$

with $k'_x \equiv k_x - \pi$. It represents an anisotropic Dirac cone. Similarly, with respect to the band with down spin $s = -1$, there is a Dirac cone at the Y point, where the Hamiltonian is expanded as

$$H_\downarrow^Y = -4C + tk'_y\tau_x - \lambda k_x\tau_y + (4B - 2u)\tau_z \quad (3)$$

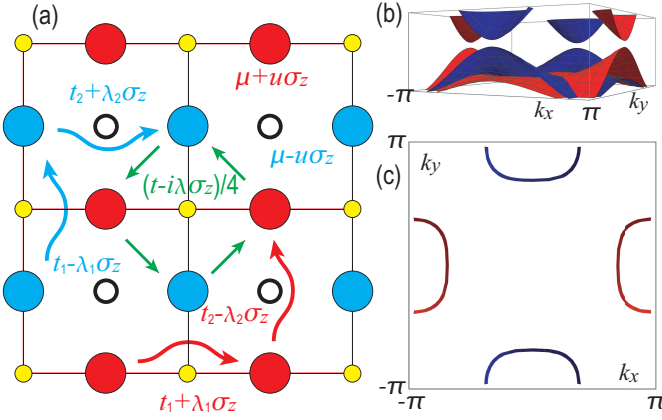


FIG. 1. (a) Illustration of the Lieb lattice model. Red (cyan) disks represent sites with up (down) spin. Small yellow disks represent non-magnetic sites. The tight-binding model is constructed only with the use of red and blue disks, where the hopping terms are modified in the presence of yellow disks. Red (cyan) arrows represent hoppings between the next-nearest neighbor up(down)-spin sites. Green arrows represent hoppings between the nearest-neighbor sites between opposite spins. We have set $A = t_1 + t_2$, $B = t_1 - t_2$, $C = \lambda_1 + \lambda_2$ and $D = \lambda_1 - \lambda_2$ in the Hamiltonian (1). (b) Bird's eye's view of the band structure containing two anisotropic Dirac cones. (c) Top view of the band structure. Red (blue) color represents the up-spin (down-spin) band structure.

with $k'_y \equiv k_y - \pi$.

The Hamiltonians H_{\uparrow}^X and H_{\downarrow}^Y are rewritten in the form of $H(\mathbf{k}) = h_0(\mathbf{k}) + \mathbf{h}(\mathbf{k}) \cdot \boldsymbol{\tau}$. The energy spectrum is obtained as

$$\varepsilon_{\pm}(\mathbf{k}) = h_0(\mathbf{k}) \pm \sqrt{|\mathbf{h}(\mathbf{k})|}. \quad (4)$$

We define the normalized vector $\mathbf{n}(\mathbf{k})$ as $\mathbf{n}(\mathbf{k}) \equiv \mathbf{h}(\mathbf{k})/|\mathbf{h}(\mathbf{k})| = (\sin \theta \cos \phi, \sin \theta \sin \phi, \cos \theta)$. The quantum metric for the two-band system is explicitly given[41–48] by $g_{\pm}^{\mu\nu}(\mathbf{k}) = \pm \frac{1}{4} (\partial_{k_{\mu}} \mathbf{n}) \cdot (\partial_{k_{\nu}} \mathbf{n})$ with the normalized vector $\mathbf{n}(\mathbf{k})$.

The Berry curvature for the two-band system is explicitly given[41, 44, 49–51] by $\Omega_{\pm}^{xy}(\mathbf{k}) = \mp \frac{1}{2} \mathbf{n} \cdot (\partial_{k_x} \mathbf{n} \times \partial_{k_y} \mathbf{n})$. It is a solid angle spanned by the vector \mathbf{n} . The quantum metrics $g_{xx}^X(\mathbf{k})$, $g_{yy}^X(\mathbf{k})$ and the Berry curvature $\Omega_{xy}^X(\mathbf{k})$ at the X point are given by

$$g_{xx}^X(k'_x, k_y) = \frac{t^2 \left((\lambda k_y)^2 + \Delta^2 \right)}{4 \left((t k'_x)^2 + (\lambda k_y)^2 + \Delta^2 \right)^2}, \quad (5)$$

$$g_{yy}^X(k'_x, k_y) = \frac{\lambda^2 \left((t k'_x)^2 + \Delta^2 \right)}{4 \left((t k'_x)^2 + (\lambda k_y)^2 + \Delta^2 \right)^2}, \quad (6)$$

$$\Omega_{xy}^X(k'_x, k_y) = \frac{\Delta t \lambda}{2 \left((t k'_x)^2 + (\lambda k_y)^2 + \Delta^2 \right)^{3/2}} \quad (7)$$

with the Dirac mass $\Delta = 4B - 2u$. Similarly, we have

$$g_{xx}^Y(k_x, k'_y) = g_{xx}^X(k'_x, k_y), \quad (8)$$

$$g_{yy}^Y(k_x, k'_y) = g_{yy}^X(k'_x, k_y), \quad (9)$$

$$\Omega_{xy}^Y(k_x, k'_y) = \Omega_{xy}^X(k'_x, k_y) \quad (10)$$

at the Y point. The integration of the Berry curvature gives the half-quantized Chern number for a single Dirac cone,

$$\frac{1}{2\pi} \int \Omega_{xy}^X(\mathbf{k}) d\mathbf{k} = \frac{1}{2\pi} \int \Omega_{xy}^Y(\mathbf{k}) d\mathbf{k} = \frac{\Delta}{2|\Delta|}. \quad (11)$$

By summing up two Chern numbers from the two Dirac cones, we obtain a quantized Chern number,

$$\frac{1}{2\pi} \int (\Omega_{xy}^X(\mathbf{k}) + \Omega_{xy}^Y(\mathbf{k})) d\mathbf{k} = \frac{\Delta}{|\Delta|}. \quad (12)$$

It shows that the system is a Chern insulator, where quantum anomalous Hall effects occur.

Elliptic optical dichroism: We next analyze optical absorption. We apply elliptically polarized light with the electric field

$$\mathbf{E}(\omega) = E(\omega) (\mathbf{e}_x \cos \vartheta + i \mathbf{e}_y \sin \vartheta), \quad (13)$$

where ϑ is the ellipticity of injected light $0 < \vartheta < \pi$ for the right polarization, and $-\pi < \vartheta < 0$ for the left polarization. $\vartheta = \pi/4$ corresponds to the right circularly polarized light, while $\vartheta = -\pi/4$ corresponds to the left circularly polarized light. The optical conductivity is calculated as[8, 15]

$$\sigma(\omega; \vartheta) = \hbar^2 \sigma_0 \int d\mathbf{k} f(\mathbf{k}) g(\mathbf{k}; \vartheta) \delta[\varepsilon_+(\mathbf{k}) - \varepsilon_-(\mathbf{k}) - \hbar\omega] \quad (14)$$

with

$$g(\mathbf{k}; \vartheta) \equiv g_{xx}(\mathbf{k}) \cos^2 \vartheta + g_{yy}(\mathbf{k}) \sin^2 \vartheta + \Omega_{xy}(\mathbf{k}) \sin \vartheta \cos \vartheta, \quad (15)$$

where $g_{xx}(\mathbf{k})$ and $g_{yy}(\mathbf{k})$ are quantum metrics and $\Omega_{xy}(\mathbf{k})$ is the Berry curvature. The detailed derivation is shown in Supplemental Material. We denote Eq.(15) by $g^X(\mathbf{k}; \vartheta)$ at the X point and $g^Y(\mathbf{k}; \vartheta)$ at the Y point. It is observed from Eq.(14) that the minimum of the excitation frequency ω is given by the optical band edge $\hbar\omega = 2|\Delta|$, where excitation occurs at the X or Y point: See Fig.2(a). There is no optical absorption below the optical band edge.

We calculate Eq.(14) based on the Dirac model around the X and Y points. Namely, we set $\mathbf{k} = (k'_x, k_y)$ at the X point and $\mathbf{k} = (k_x, k'_y)$ at the Y point. After integrating the momentum integration, we obtain

$$\sigma(\omega; \vartheta) = \hbar^2 \sigma_0 \int \frac{k_{\text{FG}}(k_{\text{F}})}{|\partial_k \varepsilon(k)|_{k_{\text{F}}}} d\phi = \frac{2\hbar^2 \sigma_0}{\omega} \int_0^{2\pi} g(k_{\text{F}}) d\phi, \quad (16)$$

where $k_{\text{F}} = \sqrt{(\hbar\omega/2)^2 - \Delta^2}$ is the solution of $\hbar\omega = \varepsilon_+(k_{\text{F}}) - \varepsilon_-(k_{\text{F}})$. We have set $k_x = k \cos \phi$, $k_y = k \sin \phi$, and used $\partial_k \varepsilon(k) = k/\sqrt{k^2 + \Delta^2}$. The optical conductivity at the optical band edge $\hbar\omega = 2|\Delta|$ is given by

$$\sigma(\omega = 2|\Delta|; \vartheta) = \frac{\hbar^3 \sigma_0}{|\Delta|} g(\mathbf{0}; \vartheta), \quad (17)$$

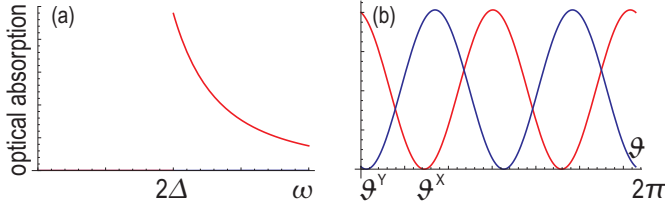


FIG. 2. (a) Optical absorption as a function of ω . Red (blue) curve corresponds to the spin up (down) polarization. We have set $\vartheta = \vartheta^Y$, where only electrons with up spin is excited. (b) Optical absorption as a function of ϑ at the optical band edge $\hbar\omega = 2|\Delta|$. We have set $t = 4$; $\lambda = 0.5$; $B = -1$ and $u = -2.2$.

where we have used $k_F = 0$ at the optical band edge.

The condition that no electrons are excited at the Y point is given by

$$g^Y(\mathbf{0}; \vartheta^Y) = 0. \quad (18)$$

By solving this equation, the ellipticity of the light ϑ^Y is explicitly determined as

$$\vartheta^Y = \arccos \frac{t}{\sqrt{\lambda^2 + t^2}}. \quad (19)$$

Then, it follows from Eq.(15) and Eq.(17) that the optical conductivity at the optical band edge $\omega = 2|\Delta|$ is given by

$$\frac{\sigma^X(\omega = 2|\Delta|; \vartheta^Y)}{\hbar^3 \sigma_0 / |\Delta|} = \frac{2|\Delta| t^2 \lambda |\lambda| + \Delta(\lambda^4 + t^4)}{2\Delta^3(\lambda^2 + t^2)}, \quad (20)$$

implying that electrons are excited at the X point. Hence, elliptic optical dichroism occurs.

In general, the ω dependence of the optical conductivity is obtained as

$$\frac{\sigma^Y(\omega; \vartheta^Y)}{\hbar^2 \sigma_0} = \frac{\pi \lambda t (\hbar\omega + 2\Delta)}{(\hbar\omega)^3 (\lambda^2 + t^2)} \quad (21)$$

around the Y point, and

$$\frac{\sigma^X(\omega; \vartheta^Y)}{\hbar^2 \sigma_0} = \frac{\pi}{2\lambda t (\hbar\omega)^3 (\lambda^2 + t^2)} \times (4\Delta^2 (\lambda^4 + t^4) + 8\Delta \hbar\omega \lambda^2 t^2 + \hbar^2 \omega^2 (t^4 + \lambda^4)) \quad (22)$$

around the X point. The optical conductivity is shown as a function of ω in Fig.2(a). The optical conductivity takes the maximum value (20) at the optical band edge $\omega = 2|\Delta|$ and monotonically decreases $\sigma^X(\omega; \vartheta^Y) \propto 1/\omega$ as the increase of ω .

Similarly, no electrons are excited at the X point if

$$g^X(\mathbf{0}; \vartheta^X) = 0 \quad (23)$$

with

$$\vartheta^X = \arccos \frac{\lambda}{\sqrt{\lambda^2 + t^2}}, \quad (24)$$

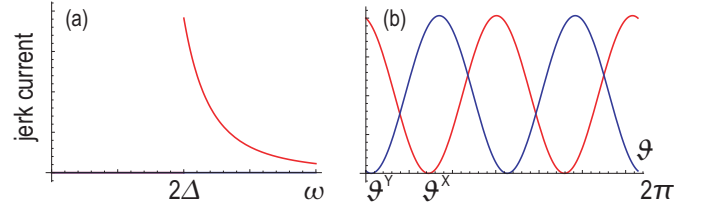


FIG. 3. (a) Jerk current as a function of ω dependence Red (blue) curve corresponds to the spin up (down) polarization. We have set $\vartheta = \vartheta^Y$, where only electrons with up spin is excited. (b) Jerk current as a function of ϑ at the optical band edge $\hbar\omega = 2|\Delta|$.

where the optical conductivity at the optical band edge is given by

$$\sigma(\omega = 2|\Delta|; \vartheta^X) = \hbar^2 \sigma_0 G^Y(\mathbf{0}; \vartheta^X) \quad (25)$$

with

$$g^Y(\mathbf{0}; \vartheta^X) = \frac{2|\Delta| \lambda^2 t |t| + \Delta(\lambda^4 + t^4)}{2\Delta^3(\lambda^2 + t^2)}. \quad (26)$$

The optical conductivity is shown as a function of ϑ at the optical band edge in Fig.2(b).

It is possible to make $g^Y(\mathbf{0}; \vartheta^Y) = 0$ or $g^X(\mathbf{0}; \vartheta^X) = 0$ by tuning the ellipticity of irradiated light ϑ , where only electrons at the X point or the Y point are selectively excited. It is elliptic optical dichroism.

Jerk current under elliptically polarized light: We now show that these excited electrons are extracted by applying electric field additionally. The second-order photocurrents such as the injection current[16–25] and the shift current[16–20, 23–33] are zero due to inversion symmetry. On the other hand, the third-order photocurrent[34–38] is not prohibited by the presence of inversion symmetry. The higher-order injection current was derived for the linearly polarized light[38]. We generalize it to elliptically polarized light, where the ℓ -th order photocurrent is given by

$$J^{x;x^\ell}(\omega) = \frac{\ell - 1}{(i\omega_0 + 1/\tau)^{\ell-1}} \frac{2\pi e^{\ell+1}}{\hbar^\ell V} \int d\mathbf{k} g(\mathbf{k}; \vartheta) \delta(\omega_{+-} - \omega) \times \frac{\partial^{\ell-1} \omega_{+-}}{\partial k_x^{\ell-1}} E(\omega) E(-\omega) [E_x(0)]^{\ell-2}, \quad (27)$$

where ω_0 is the frequency of applied electric field and $\hbar\omega_{+-} \equiv (\varepsilon_+ - \varepsilon_-)$ with Eq.(4) is the difference of the energy between the conduction and valence bands. The detailed derivation is shown in Supplemental Material.

We calculate the jerk current with $\ell = 3$ at the optical band edge, which is the leading order of photocurrent. It is obtained from Eq.(27) as

$$\frac{J^{x;x^3}(\Delta; \vartheta^Y)}{(i\omega_0 + 1/\tau)^2 \frac{2\pi e^4}{\hbar^3 V} E(\omega) E(-\omega) E_x(0)} = \frac{\pi t (\lambda^2 - t^2)^2}{2\Delta^2 \lambda (\lambda^2 + t^2)} \quad (28)$$

at the X point. This result is derived as follows. It follows from Eq.(4) that

$$\frac{\partial^2 \omega_{+-}(\mathbf{k})}{\partial k_x^2} = \frac{t^2}{\sqrt{(tk'_x)^2 + (\lambda k_y)^2 + \Delta^2}} - \frac{t^4 k_x^2}{\left((tk'_x)^2 + (\lambda k_y)^2 + \Delta^2\right)^{3/2}}, \quad (29)$$

which leads to

$$\frac{\partial^2 \omega_{+-}(\mathbf{0})}{\partial k_x^2} = \frac{t^2}{|\Delta|} \quad (30)$$

at the optical band edge. In addition, it follows from Eqs.(5), (6) and (7) that

$$g_{xx}^X(\mathbf{0}) = \frac{t^2}{4\Delta^2}, \quad g_{yy}^X(\mathbf{0}) = \frac{\lambda^2}{4\Delta^2}, \quad \Omega_{xy}^X(\mathbf{0}) = \frac{t\lambda}{2\Delta^2}. \quad (31)$$

With the use of these and Eq.(15), we obtain

$$g(\mathbf{0}; \vartheta) = \frac{t^2}{4\Delta^2} \cos^2 \vartheta + \frac{\lambda^2}{4\Delta^2} \sin^2 \vartheta + \frac{t\lambda}{2\Delta^2} \sin \vartheta \cos \vartheta. \quad (32)$$

By inserting Eq.(30) and Eq.(32) to Eq.(27), we obtain Eq.(28). It is interesting that the jerk current is zero for isotropic Dirac cone with $\lambda = t$ at the optical band edge as in Eq.(28).

In general, the ω dependence of the jerk current is explicitly given by

$$\begin{aligned} & \frac{J^{x;x^3}(\omega; \vartheta^Y)}{\frac{2}{(i\omega_0+1/\tau)^2} \frac{2\pi e^4}{\hbar^3 V} E(\omega) E(-\omega) E_x(0)} \\ &= \frac{\pi t}{4(\hbar\omega)^6 (\lambda^2 + t^2)} \\ & \times \left((\lambda^4 + 3t^4) \left((\hbar\omega)^4 + 16\Delta^4 \right) + 8\Delta^2 (3\lambda^4 + t^4) (\hbar\omega)^2 \right) \end{aligned} \quad (33)$$

at the X point, and

$$\begin{aligned} & \frac{J^{x;x^3}(\omega; \vartheta^Y)}{\frac{2}{(i\omega_0+1/\tau)^2} \frac{2\pi e^4}{\hbar^3 V} E(\omega) E(-\omega) E_x(0)} \\ &= \frac{\pi \lambda t^3 (\hbar^2 \omega^2 + 4\Delta^2) (\hbar\omega + 2\Delta)^2}{(\hbar\omega)^6 (\lambda^2 + t^2)} \end{aligned} \quad (34)$$

at the Y point.

The jerk current is shown as a function of ω in Fig.3(a), where the jerk current takes the maximum value (28) at the optical band edge $\hbar\omega = 2|\Delta|$ and monotonically decreases $J_{\text{inject}}^{x;x^3}(\omega; \vartheta^Y) \propto 1/\omega^2$ as the increase of ω . The jerk current with up spins is induced by elliptically polarized light with $\vartheta = \vartheta^Y$, while there is no jerk current with down spin at the optical band edge $\hbar\omega = 2|\Delta|$. We show the jerk current as a function of ϑ at the optical band edge in Fig.3(b). The portion of the spin polarization is controlled by tuning the ellipticity ϑ .

We note that, in the case of the isotropic Dirac cone with $\lambda = t$, the jerk current is identical at the X and Y points, and given by

$$\begin{aligned} & \frac{J^{x;x^3}(\omega; \vartheta^Y)}{\frac{2}{(i\omega_0+1/\tau)^2} \frac{2\pi e^4}{\hbar^3 V} E(\omega) E(-\omega) E_x(0)} \\ &= \frac{\pi t^2 (\hbar^2 \omega^2 + 4\Delta^2) (\hbar\omega + 2\Delta)^2}{(\hbar\omega)^6}. \end{aligned} \quad (35)$$

The jerk current is zero at the optical band edge for the isotropic Dirac cones,

$$J^{x;x^3}\left(\omega = -\frac{2\Delta}{\hbar}; \vartheta^Y\right) = 0. \quad (36)$$

Hence, the jerk current at the optical band edge is present only for anisotropic Dirac cones.

Discussions: We have shown that the low-energy theory of d -wave altermagnets is described by a model with anisotropic Dirac cones at the X and Y points, where spins are perfectly polarized to up (down) at the X (Y) point. By tuning the ellipticity of light, it is possible to selectively excite up or down spins, which is known as elliptic optical dichroism. By applying electric field in addition to the elliptically polarized light, the perfectly spin-polarized jerk current is induced. It is interesting that the jerk current is enhanced at the optical band edge only for anisotropic Dirac cones. Our work will be useful for photo-excited spintronics based on d -wave altermagnets.

This work is supported by CREST, JST (Grants No. JPMJCR20T2) and Grants-in-Aid for Scientific Research from MEXT KAKENHI (Grant No. 23H00171).

-
- [1] L. Smejkal, J. Sinova, and T. Jungwirth, Beyond Conventional Ferromagnetism and Antiferromagnetism: A Phase with Non-relativistic Spin and Crystal Rotation Symmetry, *Phys. Rev. X*, 12, 031042 (2022).
 [2] Libor Šmejkal, Jairo Sinova, and Tomas Jungwirth, Emerging Research Landscape of Altermagnetism, *Phys. Rev. X* 12, 040501 (2022).

- [3] Makoto Naka, Satoru Hayami, Hiroaki Kusunose, Yuki Yanagi, Yukitoshi Motome and Hitoshi Seo, Spin current generation in organic antiferromagnets, *Nat. Com.* 10, 4305 (2019).
 [4] Rafael Gonzalez-Hernandez, Libor Šmejkal, Karel Vborn, Yuta Yahagi, Jairo Sinova, Tomš Jungwirth, and Jakub Železn, Efficient electrical spin splitter based on nonrelativistic collinear antiferromagnetism, *Phys. Rev. Lett.*, 126:127701, (2021).

- [5] M Naka, Y Motome, and H Seo, Perovskite as a spin current generator. *Phys. Rev. B*, 103, 125114, (2021).
- [6] Arnab Bose, Nathaniel J. Schreiber, Rakshit Jain, Ding-Fu Shao, Hari P. Nair, Jiaxin Sun, Xiyue S. Zhang, David A. Muller, Evgeny Y. Tsymbal, Darrell G. Schlom & Daniel C. Ralph, Tilted spin current generated by the collinear antiferromagnet ruthenium dioxide, *Nature Electronics* 5, 267 (2022).
- [7] Makoto Naka, Yukitoshi Motome and Hitoshi Seo, Altermagnetic Perovskites, *npj Spintronics* 3, 1 (2025)
- [8] Motohiko Ezawa, Quantum geometry and X-wave magnets with $X=p,d,f,g,i$, arXiv:2512.05477 to be published in APEX.
- [9] Zesen Fu, Mengli Hu, Aolin Li, Haiming Duan, Junwei Liu, Fangping Ouyang, Multiple Topological Phases Controlled via Strain in Two-Dimensional Altermagnets, arXiv:2507.22474
- [10] W. Yao, D. Xiao, and Q. Niu, *Phys. Rev. B* 77, 235406 (2008).
- [11] D. Xiao, G.-B. Liu, W. Feng, X. Xu, and W. Yao, Coupled Spin and Valley Physics in Monolayers of MoS₂ and Other Group-VI Dichalcogenides, *Phys. Rev. Lett.* **108**, 196802 (2012).
- [12] M. Ezawa, Spin-valley optical selection rule and strong circular dichroism in silicene, *Phys. Rev. B* 86, 161407(R) (2012)
- [13] X. Li, T. Cao, Q. Niu, J. Shi, and J Feng, Coupling the valley degree of freedom to antiferromagnetic order, *PNAS* 110 (10) 3738 (2013)
- [14] M. Ezawa, Elliptic Dichroism and Valley-Selective Optical Pumping in the Surface of Topological Crystalline Insulator, *Phys. Rev. B* 89, 195413 (2014)
- [15] M. Ezawa, Quantum geometry and elliptic optical dichroism in p-wave magnets, *Phys. Rev. B* 112, 045302 (2025)
- [16] J. E. Sipe and A. I. Shkrebti, Second-order optical response in semiconductors, *Phys. Rev. B* 61, 5337 (2000).
- [17] C. Aversa and J. E. Sipe, Nonlinear Optical Susceptibilities of Semiconductors: Results with a Length-Gauge Analysis, *Phys. Rev. B* 52, 14636 (1995)
- [18] J. Ahn, G.-Y. Guo, N. Nagaosa, Low-Frequency Divergence and Quantum Geometry of the Bulk Photovoltaic Effect in Topological Semimetals, *Phys. Rev. X* 10, 041041 (2020).
- [19] J. Ahn, G.-Y. Guo, N. Nagaosa, A. Vishwanath, Riemannian geometry of resonant optical responses, *Nature Physics* 18, 290 (2022)
- [20] F. de Juan, Y. Zhang, T. Morimoto, Y. Sun, J. E. Moore, and A.G. Grushin, Difference Frequency Generation in Topological Semimetals, *Phys. Rev. Research* 2, 012017 (2020).
- [21] Fernando de Juan, Adolfo G. Grushin, Takahiro Morimoto, Joel E. Moore, Quantized circular photogalvanic effect in Weyl semimetals, *Nature Communications* 8, 15995 (2017).
- [22] Shun Okumura, Takahiro Morimoto, Yasuyuki Kato, and Yukitoshi Motome, Quadratic optical responses in a chiral magnet, *Phys. Rev. B* 104, L180407 (2021)
- [23] Hikaru Watanabe and Youichi Yanase, Chiral Photocurrent in Parity-Violating Magnet and Enhanced Response in Topological Antiferromagnet, *Phys. Rev. X*, 11, 011001 (2021)
- [24] Z. Dai and A. M. Rappe, Recent progress in the theory of bulk photovoltaic effect, *Chemical Physics Reviews* 4, 011303 (2023).
- [25] M. Ezawa, Bulk photovoltaic effects in altermagnets, *Phys. Rev. B* 111, L201405 (2025)
- [26] W. Kraut and R. von Baltz, Anomalous bulk photo-voltaic effect in ferroelectrics: A quadratic response theory, *Phys. Rev. B* 19, 1548 (1979).
- [27] V. Baltz, A. Manchon, M. Tsoi, T. Moriyama, T. Ono, and Y. Tserkovnyak, Antiferromagnetic spintronics, *Rev. Mod. Phys.* 90, 015005 (2018).
- [28] S. M. Young and A. M. Rappe, First Principles Calculation of the Shift Current Photovoltaic Effect in Ferroelectrics, *Phys. Rev. Lett.* 109, 116601 (2012).
- [29] S. M. Young, F. Zheng, and A. M. Rappe, First-Principles Calculation of the Bulk Photovoltaic Effect in Bismuth Ferrite, *Phys. Rev. Lett.* 109, 236601 (2012).
- [30] T. Morimoto and N. Nagaosa, Topological nature of nonlinear optical effects in solids, *Science Advances* 2, e1501524 (2016)
- [31] Kun Woo Kim, Takahiro Morimoto, and Naoto Nagaosa, Shift charge and spin photocurrents in Dirac surface states of topological insulator, *Phys. Rev. B*, 95, 035134 (2017)
- [32] T. Barik and J. D. Sau, Nonequilibrium nature of nonlinear optical response: Application to the bulk photovoltaic effect, *Phys. Rev. B* 101, 045201 (2020).
- [33] Hiroki Yoshida and Shuichi Murakami, Diverging shift current responses in the gapless limit of two-dimensional systems, *Phys. Rev. B* 111, 155402 (2025)
- [34] B. M. Fregoso, R. A. Muniz and J.E. Sipe, Jerk Current: A Novel Bulk Photovoltaic Effect, *Phys. Rev. Lett.* 121, 176604 (2018)
- [35] G. B. Ventura, D.J. Passos, J. M. Viana Parente Lopes, and J. M. B. Lopes dos Santos, Comment on "Jerk Current: A Novel Bulk Photovoltaic Effect" *Phys. Rev. Lett.* 126, 259701 (2021)
- [36] B. M. Fregoso, R. A. Muniz and J.E. Sipe, "Fregoso, Muniz, and Sipe Reply" *Phys. Rev. Lett.* 126, 259702 (2021)
- [37] Benjamin M. Fregoso, Bulk photovoltaic effects in the presence of a static electric field, *Phys. Rev. B* 100, 064301 (2019): Erratum, *Phys. Rev. B* 102, 059901(E) (2020)
- [38] M. Ezawa, Higher-order bulk photovoltaic effects, quantum geometry and application to p-wave magnets, *Phys. Rev. B* 112, 155308 (2025)
- [39] D. S. Antonenko, R. M. Fernandes, and J. W. F. Venderbos, Mirror chern bands and weyl nodal loops in altermagnets, *Phys. Rev. Lett.* 134, 096703 (2025)
- [40] P. Feng, C.-Y. Tan, M. Gao, X.-W. Yan, Z.-X. Liu, P.-J. Guo, F. Ma, and Z.-Y. Lu, Type-II quantum spin hall insulator, arXiv:2503.13397
- [41] O. Bleu, D. D. Solnyshkov, and G. Malpuech, Measuring the quantum geometric tensor in two-dimensional photonic and exciton-polariton systems, *Phys. Rev. B* 97, 195422 (2018)
- [42] Shunji Matsuura and Shinsei Ryu, Momentum space metric, nonlocal operator, and topological insulators, *Phys. Rev. B* 82, 245113 (2010)
- [43] G. von Gersdorff and W. Chen, Measurement of topological order based on metric-curvature correspondence, *Phys. Rev. B* 104, 195133 (2021).
- [44] Y.-M. Robin Hu, Elena A. Ostrovskaya, and Eliezer Estrecho, Generalized quantum geometric tensor in a non-Hermitian exciton-polariton system, *Optical Materials Express* 14, 664 (2024)
- [45] Yugo Onishi and Liang Fu, Fundamental Bound on Topological Gap, *Phys. Rev. X* 14, 011052 (2024)
- [46] Wei Chen, Quantum geometrical properties of topological materials, *J. Phys.: Condens. Matter* 37 025605 (2025)
- [47] M. Ezawa, Analytic approach to quantum metric and optical conductivity in Dirac models with parabolic mass in arbitrary dimensions, *Phys. Rev. B* 110, 195437 (2024)
- [48] Chang-geun Oh, Sun-Woo Kim, Kun Woo Kim, Bartomeu Monserrat, and Jun-Won Rhim, Universal Optical Conductivity from Quantum Geometry in Quadratic Band-Touching Semimetals, arXiv:2503.18372
- [49] W.-Y. Hsiang and D.-H. Lee, Chern-Simons invariant in the Berry phase of a 2×2 Hamiltonians, *Phys. Rev. A* 64, 052101 (2001).
- [50] Doru Sticlet, Frederic Piechon, Jean-Noel Fuchs, Pavel Kalugin, and Pascal Simon, Geometrical engineering of a two-band

Chern insulator in two dimensions with arbitrary topological index, Phys. Rev. B 85, 165456 (2012).

[51] Chao-Ming Jian, Zheng-Cheng Gu, and Xiao-Liang Qi, Momentum-space instantons and maximally localized flat-band

topological Hamiltonians, Phys. Status Solidi RRL 7, 154 (2013)